BİTLİS EREN ÜNİVERSİTESİ
FEN BİLİMLERİ DERGİSİ

ISSN: 2147-3129 / e-ISSN: 2147-3188

Article Type	: Research Article	**Year**	: 2025
Received	: August 7, 2024	**Volume**	: 14
Revised	: February 20, 2025	**Issue**	: 1
Accepted	: March 5, 2025	**Pages**	: 13-38
DOI	: 10.17798/bitlisfen.1518320		

PERFORMANCE COMPARISONS OF THERMAL PROTECTION METHODS BASED ON THERMALLY ENHANCED PHASE CHANGE MATERIALS

Ahmet Can ÇAPAR[1], **Ümit Nazlı TEMEL[2*]**

[1] *Turkish Electricity Transmission Corporation, Sivas, Türkiye*

[2] *Sivas Cumhuriyet University, Mechanical Engineering Department, Sivas, Türkiye*

**** Corresponding Author:*** untemel@cumhuriyet.edu.tr

ABSTRACT

This study focuses on phase change material-based passive thermal protection of electronic components that release heat for a period of time. Firstly, an investigation was carried out in terms of PCM thickness for thermal protection and it was determined that an 11 mm thickness was the appropriate PCM thickness. It was determined that the thermal conductivities in the solid phase could be improved by 35.9%, 119.2%, and 178.6%, respectively, if 1%, 3%, and 5% GNP were doped into the PCM. In the case of 1%, 3%, and 5% GNP doping, it was determined that the melting temperatures of PCM did not change, whereas the latent heat of melting decreased slightly depending on the GNP fraction. The deterioration in the latent melting heat for 5% GNP/RT-44 composite was measured as 5.4%. Then, the thermal protection performance of PCM, Fin/PCM, Nanoparticle/PCM, and Nanoparticle/Fin/PCM composites on an electronic component that releases heat for a period of time was compared in terms of maximum surface temperature and maximum surface temperature difference. The results indicated that the Nanoparticle/PCM thermal protection exhibited a performance improvement effect predominantly during sensible heat storage, whereas the Fin/PCM thermal protection demonstrated an improvement in performance during both sensible heat and latent heat storage. While all thermal protection methods were successful at 3 W heating power, only PCM thermal protection equipped with six fins (6F/PCM) was successful at 6W heating power. At 6 W heating power, maximum temperature and maximum temperature difference performances were improved by 15.3% and 45.2%, respectively, with 6F/PCM thermal protection compared to PCM thermal protection only. An increase in the GNP mass fraction above 3% has been demonstrated to have a detrimental effect on thermal protection. With 3% GNP/6F/PCM hybrid thermal protection, it was determined that the maximum temperature and maximum temperature difference performances have the potential to be improved by 22.3% and 53.4% compared to PCM thermal protection.

Keywords: PCM, Thermal protection, Fin, Nanoparticles, Hybrid thermal protection

ABBREVIATIONS

PCM	: Phase Change Material	**CNTs**	: Carbon Nano Tubes
GNP	: Graphene Nano Platelets	**BN**	: Boron Nitride
PW	: Paraffin Wax	**EG**	: Expanded Graphite
LA	: Lauric Acit	**FLG**	: Few Layer Graphene
MWCNTs	: Multi-Walled Carbon Tubes	**PEG**	: Polyethylene Glycol
S-MWCNTs	: Short MWCNTs	**DSC**	: Differential Scanning Calorimetry
L-MWCNTs	: Long MWCNTs	**DC**	: Direct Current
CNFs	: Carbon Nano Fiber	**SiC**	: Silicone Carbide

1 INTRODUCTION

Phase change materials (PCMs) have the potential to store thermal energy due to their high latent heat. The heat absorbed from a source is stored thermally as the PCM transitions to a higher energy state during the phase change process. Conversely, the PCM releases the stored thermal energy as it returns to a lower energy state during the reverse phase change. With this feature, PCMs have a wide range of applications such as energy storage in solar panels [1] and building walls [2], thermal protection of electronic devices [3], performance improvement of coolers [4], waste heat recovery [5] and blood and organ transplantation [6].

The thermal energy released by transient electronic devices during operation leads to an undesired temperature increase within the device. This temperature rise can cause the device to malfunction or operate inefficiently. Therefore, it is essential to thermally protect transient operating devices by effectively dissipating the thermal energy they generate for instance, during the transient operation of battery cells, it is crucial to maintain the maximum temperature below 50 °C and the maximum temperature difference below 5 °C. Failure to do so may result in issues such as explosion risks, capacity loss, short charge/discharge cycles, and accelerated aging of the battery cells. Passive thermal protection of transient electronic devices based on the use of PCM is seen as an innovative method because it is economical and does not involve moving mechanical systems such as pumps and fans. The effectiveness of this type of thermal protection depends on the rapid transfer of the heat released in electronic devices to the PCM. In other words, the PCM used must have a rapid thermal response. This outcome necessitates a high thermal conductivity for PCM. Conversely, the thermal conductivity of PCMs that are suitable for practical applications is relatively low. This is the most important obstacle to the use of PCMs in the thermal protection of electronic devices. To enable the use of PCMs for passive thermal protection, enhancing their heat transfer capabilities is essential. Efforts to

improve the thermal conductivity of PCMs can be grouped into three main categories. The first involves creating PCM/nanoparticle composites by incorporating nanoparticles with high thermal conductivity into the PCM. The second method uses thermal bridges, such as metal fins or pins, embedded in the PCM to enhance heat dissipation. The third approach entails forming shape-stable composites by impregnating PCM into the pores of highly porous materials. A comparative analysis of these thermal protection methods is presented in Table 1.

Table 1. Comparative literature studies.

Ref.	Composite	Proportion	Melting Temp. of PCM (°C)	Latent Heat (J/g) PCM – PCM/Additive	Thermal Cond. (W/mK) or Enhancement (%) PCM – PCM/Additive	Load	T_{max} (°C)	ΔT_{max} (°C)
Chinnasamy et al. [7]	LA – LA/CuO, LA/Fe_3O_4, LA/SiC, LA/Al_2O_3	95%/5%	22.1	217 – 193.4, 185.3, 191.1, 185.3	0.4 – 52.2%, 9.8%, 17.9%, 29.1%	-	-	-
Temel et al. [8]	A82 – A82/ZnO, A82/TiO_2, A82/Al_2O_3, A82/MgO, A82/MWCNTs, A82/GNP	95%/5%	70.8	159 – 229, 147, 148, 139, 149, 150	0.31– 2.6%, 3.6%, 6.5%, 8.4%, 26.7%, 155%	-	-	-
Fan et al. [9]	PW – PW/S-MWCNTs, PW/L-MWCNTs, PW/CNFs, PW/GNPs	95%/5%	58.8	207 – 178, 177, 185, 187	0.263 – 23%, 17%, 16%, 166%	-	-	-
Goli et al. [10]	PW – PW/Hybride Graphene	80%/20%	-	-	0.25 – 45 (W/mK)	5A	43	13
Grosu et al. [11]	PW – PW/Cu-Mg-Zn	50%/50%	46.7	72.2 –	0.5 – 2.11 (W/mK)	2C	32.5	7.8
Zang et al. [12]	PW – PW/CNTs/BN	69%/1%/30%	52.5	150 – 60.7	0.24 – 0.69 (W/mK)	2C	52.8	-
Zou et al. [13]	PW – PW/Graph./MWCNTs/ EG		46.1	224.8– 178.5	0.38 – 5.1 (W/mK)	3C	44.6	0.8
Jiang et al. [14]	PW – PW/EG	70%/30%	42.9	275– 193	0.2 – 13.9 (W/mK)	5C	44	-
Chen et al. [15]	PW – PW/EG/FLG/GNP	88%/9%/1%/ 2%	54.5	210–179.5	0.28-0.74 (W/mK)	2C	48.9	2.1
Ma et al. [16]	Docasane – Docasane/Cu/EG	83.3%/2%/ 14.7%	43.9	205	1.18– 1.98 (W/mK)	2C	45.6	0.8
Xu et al. [17]	PW – PW/GNP/EG	76% /5%/19%	53.1	207 – 159.1	–	15W	60	-
Chen et al. [18]	PW – PW/SiC/EG	80%/10%/ 10%	45.5	155 – 122	0.28 – 4.09 (W/mK)	2C	39.3	7.8
Zhang et al. [19]	PW – PW/EG/Kaolin	80%/10% /10%	41.6	210.9– 165.2	0.40 – 7.5 (W/mK)	2C	40	3.5
Wang et al. [20]	PW – PW/Al foam	-	-	-	-	1C	26.1	-
Hussain et al. [21]	PW – PW/Nickel foam	-	-	-	0.2 – 1.16 (W/mK)	1.5C	41	0.8
Rao et al. [22]	PW – PW/Cu foam	-	37	180	0.2 – (W/mK)	5C	42	4.1
Dey et al. [23]	PEG – PEG/Al Fin	2 Fin	-	-	-	4C	34	0.8
Heyhat et al. [24]	n-Eicosane – n-Eicosane/Cu Fin	5 Fin	36.5	-	0.42 – (W/mK)	9.2 W	73	5
Moaveni et al. [25]	RT-44 – RT-44/Al Fin	4 Fin	41	270	0.2 – (W/mK)	4C	61	-
Wang et al. [26]	PW – PW/Al Fin	8 Fin	41	255	0.15 – (W/mK)	8W	52	-

In the literature, it has been shown that the low thermal conductivity of PCMs can be improved by doping metal/metal oxide nanoparticles at certain percentages. Chinnasamy et al. [7] reported enhancements in the thermal conductivity of PCM doped with 5% by mass of Al_2O_3, CuO, Fe_3O_4, and SiC nanoparticles as 29.1%, 52.2%, 9.8%, and 17.9%, respectively. In contrast, improvements in the thermal conductivity of PCMs doped with carbon-based nanoparticles have been reported to reach several-fold increases [8]. However, it is also known that the shape of the carbon-based nanoparticles plays a critical role in determining the effectiveness of the thermal conductivity improvement. Fan et al. [9] found that plate-shaped nanoparticles offer better improvements compared to tube- or thread-shaped nanoparticles. Similarly, Temel et al. [8] demonstrated that doping with 5% multi-walled carbon nanotubes resulted in a 26.7% increase in PCM thermal conductivity, while graphene nanoparticle doping at the same concentration achieved a remarkable 155% improvement.

In the literature, studies on the use of PCM/Nanoparticle composites for thermal protection purposes are generally focused on the thermal protection of batteries. When Table 1 is examined, the protection performances have been improved with thermally improved composites by doping different types of nanoparticles into paraffin type PCM. It is seen that the studies carried out in recent years are generally orientated towards the doping of more than one nanoparticle into paraffin as a hybrid. Zang et al. [12] doped carbon nanotubes (CNTs) and boron nitride (BN) within paraffin, Zou et al. [13] doped graphene (GNP), multi-walled carbon nanotubes (MWCNTs) and expanded graphite (EG) within paraffin, Chen et al. [18] doped EG and silicon carbide (SiC) in paraffin and investigated the thermal protection performances of the composite obtained by doping in terms of maximum temperature and maximum temperature difference. Similarly, Chen et al. [15] doped expanded graphite (EG), graphene nanoparticles (GNP) and few-layer graphene (FLG) hybrid nanoparticles into paraffin. They measured the maximum temperature and maximum temperature difference of the battery cell as 48.9 ^{o}C and 2.1 ^{o}C at 2C discharge rate. The most significant drawbacks of this approach are the high cost of nanoparticles and the adverse impact of enhanced liquid PCM viscosity following nanoparticle doping on heat transfer.

Another method discussed in the literature for the thermal protection of electronic components is the use of composites made by encapsulating PCM in the pores of porous structures with high thermal conductivity. Metal foams such as aluminium, nickel and copper are commonly used as base materials for this purpose. The thermal protection performance of these materials, which combine high thermal conductivity with heat storage capacity, is

summarised in Table 1. Wang et al. [20] reported that the maximum temperature for aluminum foam/paraffin composite was 26.1 ºC at 1C discharge rate. Similarly, Hussain et al. [21] reported that nickel foam/paraffin composite can maintain the maximum temperature at 41 ºC and the maximum temperature difference at 0.8 ºC at a discharge rate of 1.5C. Rao et al. [22] determined the maximum temperature and temperature difference of copper foam/paraffin composite as 42 ºC and 4.1 ºC, respectively, at a higher discharge rate of 5C. Based on the discharge rates, it is clear that aluminium and copper foams provide better thermal protection than nickel foam due to their superior thermal conductivity. While this method provides effective thermal protection, its utility is limited by the relatively small amount of PCM that can be encapsulated within the pores, which significantly reduces the duration of its effectiveness.

In another approach, metal inserts with high thermal conductivity, such as fins and pins, have been proposed to increase the heat transfer rate from the heat source to the inner regions of the phase change material (PCM). Nevertheless, the simplicity of implementation and the relatively low cost of this approach represent significant advantages. These studies were generally carried out to compare the number of fins, fin thickness, fin angle, fin length and heating direction. Hosseinizadeh et al. [27] determined that increasing the number of fins and fin length increases the thermal energy storage performance. In a study conducted by Acır et al. [28], the effects of the number of fins and fin thickness on PCM melting performance in a top-heated thermal energy storage unit were investigated. The results demonstrated that an increase in fin number has a positive effect on melting performance, whereas an increase in fin thickness has a negative effect. Tian et al. [29] conducted a numerical study to investigate the effects of materials such as aluminum, copper, and steel used as fins in an energy storage unit on melting. They determined that aluminum is the most suitable material in terms of Nusselt number, melting time, total stored energy, stored energy per mass, and cost per stored energy. Huang et al. [30] reported that increasing the number of fins in an energy storage unit makes the temperature distribution more homogeneous. When the studies on Fin/PCM thermal protection are examined in Table 1, it is seen that the effects of heat loads and number of fins are focused. Moaveni et al. [25] reported that the protection system with 4 aluminum fins equipped in RT-44 can keep the maximum temperature around 61 ºC at 4C discharge rate. Heyhat et al. [24] reported that 5 copper finned shielding systems equipped in n-Eicosane can maintain the maximum temperature and maximum temperature difference at 73 ºC and 5 ºC, respectively, under 9.2 W heat load. Wang et al. [26] showed that the paraffin protection system with 8 aluminum fins can reduce the maximum temperature up to 52 ºC under 8 W heat load. However,

it can be said that the use of fins causes an increase in weight and prevents natural convection currents according to the placement position.

A review of the above studies reveals that various techniques have been employed to enhance the thermal performance of PCMs. It is evident that these techniques provide performance improvements depending on the specific application. However, each technique has been studied under varying conditions, including nanoparticle type and concentration, fin material and quantity, and heating load. This lack of standardization has resulted in a gap in systematic comparisons of thermal protection performance. In addition, since it is not economical to use more than one nanoparticle as hybrid thermal protection in Nanoparticle/PCM thermal protection systems, there is a need to develop a lower cost hybrid thermal protection method. However, it can be said that there are not enough studies on the systematic comparison of these methods. Therefore, this study mainly involves comparing different thermal improvement methods of PCM-based thermal protection of a transient operating and heat-releasing electronic device scenario. In order to achieve this scenario, a vertical cylindrical resistance is encased in a PCM material, which serves as a thermal protection medium. As such, the experimental setup represents a battery cell that releases heat. The thermal response of the Resistance/PCM system with respect to time was measured in response to the heat released from the resistance. The objective of this study is to compare the thermal protection capabilities of PCM materials that have undergone fins and/or nanoparticle adding. For this purpose, the thermal responses of PCM with 3, 4 and 6 fins and PCM doped with 1%, 3% and 5% Graphene Nanoparticles (GNP) were analyzed. The study also investigated the performance and usability of a more economical Nanoparticle/Fin/PCM hybrid thermal protection.

2 MATERIAL AND METHOD

RT-44 organic phase change material (PCM) commercially available from Rubitherm (Germany) was used as thermal energy storage material. The transient electronic device was represented by a cylindrical resistance with a diameter of 0.018 m and a height of 0.065 m. Consequently, a representative battery cell is constructed, which is capable of releasing heat temporarily. To provide PCM-based thermal protection, the mentioned resistance was mounted on the axis of a larger diameter and 0.1 m high acrylic tube by screwing it from the bottom side (Figure 1). Thermocouples labeled T_1, T_2, and T_3, were brought into contact with the surface to measure the temperature at three different points along the resistor. Liquid PCM was poured

into the acrylic tube surrounding the resistance and left to solidify at room temperature to form the resistance-PCM system.

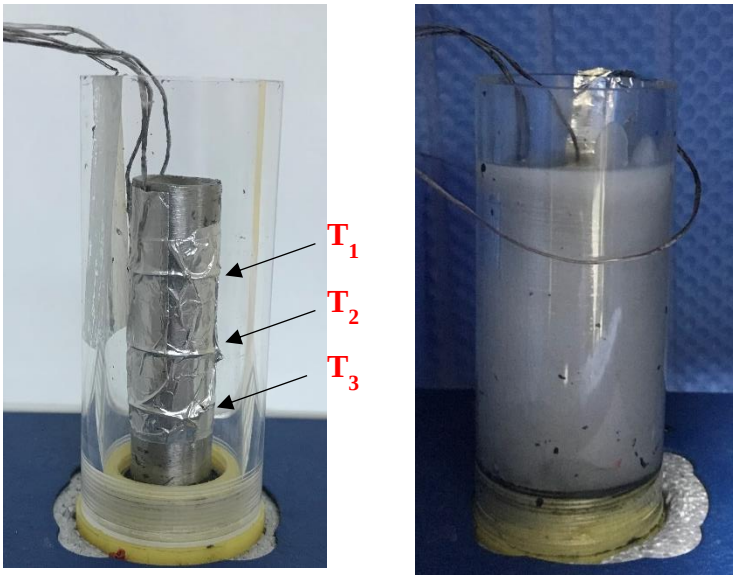

Figure 1. Resistance-PCM system.

Ping et al. [31] reported that the optimum fin thickness for thermal protection of li-ion battery cells in terms of maximum temperature and difference is 1 mm. Therefore, in this study, 1 mm thick aluminum fins were used to improve the thermal protection performance of PCM. The aluminum fins at the height of the resistance were tightly in contact with one end of the resistance, while the other end extended radially to the wall of the acrylic tube. As shown in Figure 2, different fin arrangements were realized as 3, 4 and 6 fins so that the angles between the fins were 120º (3 Fins - 3F), 90º (4 Fins - 4F) and 60º (6 Fins - 6F) respectively. Considering the studies in the literature, it is seen that variable fin numbers are used from 2 fins protection [23] to 8 fins protection [26]. Essentially, it is evident that increasing the number of fins will be effective in reducing the maximum temperature on the battery surface and achieving a more uniform temperature distribution. In their numerical study, Turkakar et al. [32] demonstrated that a 12-fin system at a 3C discharge rate maintained the average temperature on the battery surface 15 °C lower compared to the case without any thermal protection. However, the increase in the number of fins is restricted to situations where weight increase and reduction of the PCM amount are not desired. For example, for battery packs such as in this study, the increase in the number of fins should be limited due to the increase in weight. For this reason, 3, 4 and 6 fins were selected as the number of fins in this study. The resistance/Fin/PCM thermal protection system was formed by pouring the molten PCM into the acrylic tube and allowing it to solidify at room temperature.

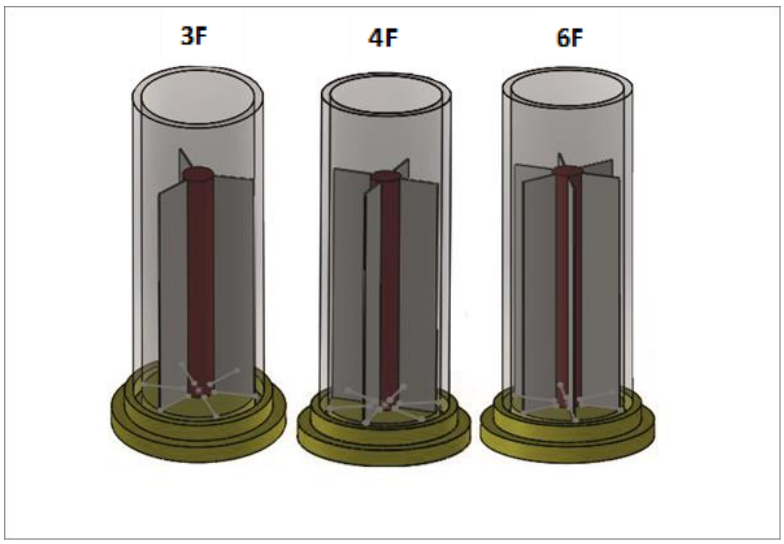

Figure 2. Fin arrangements with 3, 4 and 6 fins.

The other method used for thermal improvement in the study is the improvement of PCM low thermal conductivity with nanoparticle additives. For this purpose, plate-type GNP with high thermal conductivity and low density was used as an additive. GNP/PCM composites were synthesized by doping GNP at 1%, 3%, and 5% by mass into liquid PCM melted on a heater. The rationale for limiting the nanoparticle mass fraction to a maximum of 5% is based on the observation that an additional increase in PCM viscosity in the liquid state hurts heat transfer. The GNP nanoparticles in the PCM were mixed using a 750 W probe type ultrasonic mixer (Sonics & Materials INC, USA) for a period of 30 minutes. A mixing time of 30 minutes is sufficient to achieve a homogeneous dispersion of the nanoparticles in the PCM [33]. The resulting homogenous liquid GNP/PCM composites were poured into the region between the resistance and the tube and allowed to solidify at room temperature, thus forming a nanoparticle/PCM thermal protection system.

In this study, the thermal characterization of PCMs doped with GNP at 0% (only PCM), 1%, 3%, and 5% by mass was also obtained. For this purpose, the thermal conductivities of both PCM and GNP/PCM composites were measured using a KD2 Pro device (Decagon Devices Inc, USA) operating on the principle of transient linear heat source. Thermal conductivity measurements were carried out at different temperatures in an air conditioning cabinet (Jeiotech, South Korea) using samples prepared in accordance with the sensor inlet of the device. The accuracy of the KD2 Pro is ±0.02 W/mK for the range of 0.1-0.2 Wm/K and at least five measurements were taken for each sample and the average values were recorded with a standard deviation of 0.5%. Thermal properties such as melting temperature, latent heat of

melting was measured using a differential scanning calorimeter (DSC-60 Shimadzu Corporation, Japan). Mass-sensitive DSC samples were determined with an electronic weighing scale with an accuracy of 0.01 and samples were formed by confining them in a special container. In accordance with the expected melting temperature of the PCM used, the scan temperature range was set to 20 ºC - 60 ºC and the rate of climb was set to 2 ºC/min. The accuracy of the DSC device was 0.1 ºC and at least three measurements were performed for each sample and the average values were recorded with a standard deviation of 1%.

Thermal protection performance comparisons of differently enhanced PCMs were performed using the experimental setup shown in Figure 3. This setup consists of a DC power supply, data acquisition device, computer, air conditioning cabinet, and resistance-PCM system. The resistance-PCM systems with different thermal improvements were placed in an air conditioning cabinet and thermal response measurements were carried out under the same ambient conditions (20 ºC). The resistance was operated at 3 W and 6 W heating powers by using a DC power supply and adjusting the current to generate the heat-releasing source. Hemery et al. [34] reported that the heating powers of 0.14 W, 0.30 W, 1.30 W and 2.75 W for the resistance used as representative battery cell correspond to 0.5C, 1C, 2C and 3C discharge rates, respectively, for a real battery cell. In this case, it is clear that the selected heating powers will correspond to medium and extreme discharge rates.

Figure 3. Experimental setup used for thermal performance tests.

The temperature data at the measurement points shown in Figure 1 were measured instantaneously using J-type thermocouples. The temperature values were collected using a data logger device that measured the temperature every 30 seconds and recorded the data on a computer. The behavior of the temperatures obtained for each thermal protection method was compared with respect to time. Performance evaluations were conducted with consideration of specific criteria, including maximum temperature and maximum temperature difference. In the case of electronic components, the maximum temperature below 50 °C and the maximum temperature difference along the component below 5 °C were desired conditions.

3 RESULTS AND DISCUSSION

Temperature dependent thermal conductivity measurements for both the solid and liquid phases are shown in Figure 4. The thermal conductivity of the organic phase change material RT-44 was measured to be 0.387 W/mK at 10 °C. In the solid state, the thermal conductivity was measured to be 0.364 W/mK at 20 °C and 0.356 W/mK at 30 °C. This slight decrease in thermal conductivity can be attributed to the increase in molecular disorder with increasing temperature. At 40 °C the thermal conductivity could not be measured due to the inability of RT-44 to maintain a stable form. Upon transitioning to the liquid phase, disruptions in molecular order, such as the breakdown of lattice structures, result in a sharp decrease in thermal conductivity. The thermal conductivity values in the liquid state were recorded as 0.153 W/mK, 0.151 W/mK, and 0.148 W/mK at 50 °C, 60 °C, and 70 °C, respectively. This indicates a 59% reduction in thermal conductivity during the phase transition from solid to liquid for RT-44. A similar result was obtained in another study [35] for RT-64 with a reduction of around 41%.

The phenomenon of thermal conductivity is dependent upon the process of phonon scattering, which is in turn influenced by the lattice size and the vibrational frequency of the crystals in question. The low vibrational frequency of PCM results in a reduction in thermal conductivity, whereas the high vibrational frequency of GNP gives rise to an increase in thermal conductivity. Phonon scattering occurs along the GNP plane, rather than perpendicular to it [36]. It can thus be posited that the formation of network structures comprising the combination of GNP planes in PCM with low thermal conductivity will result in an enhancement of thermal conductivity. The formation of these network structures is directly proportional to the ratio of GNP doped into the PCM. For instance, the thermal conductivity of PCMs doped with 1%, 3%, and 5% GNP in the solid phase at 20 °C exhibited 35.9%, 119.2%, and 178.6% improvements, respectively. Similarly, enhancements of 18.5%, 55.6%, and 89.5% were observed in the

thermal conductivities of PCMs doped with 1%, 3%, and 5% GNP for the liquid phase at 50 °C, respectively. It can be reasonably assumed that similar improvements would be observed at other temperatures for both the solid and liquid phases. It was noted that the results were consistent with those reported in the literature. Kim et al. [37] achieved a 207% improvement in the solid state thermal conductivity of a 7% xGNP/PCM composite.

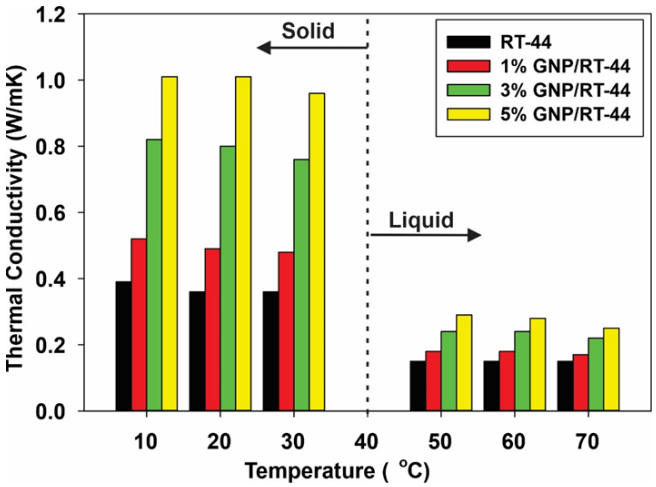

Figure 4. Thermal conductivity coefficients of RT-44 and GNP/RT-44 composites.

The DSC properties of RT-44 and GNP/RT-44 (1%, 3% and 5%) composites such as onset melting temperature (T_{om}), endset melting temperature (T_{em}), and melting latent heat (H_m) were determined by analyzing the endotherm curves given in Figure 5. The separation and junction points of these curves from the baseline give the onset melting temperature (T_{om}) and endset melting (T_{em}) temperatures, respectively. The area between the endotherm curve and the baseline is a measure of the melting latent heat of melt (H_m).

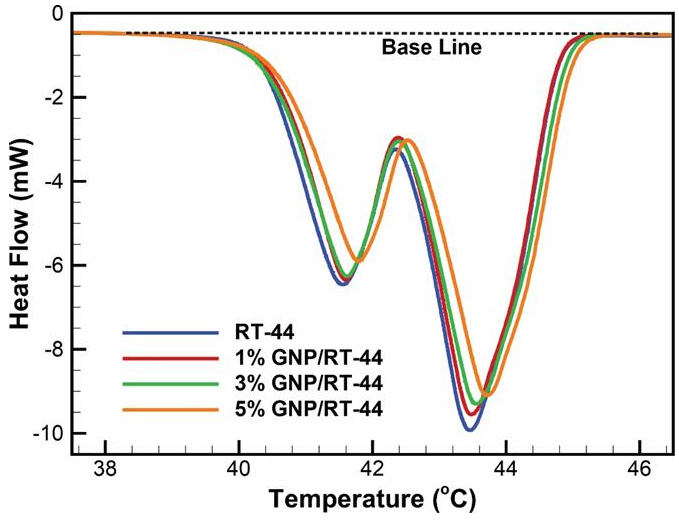

Figure 5. The endotherm curves of the RT-44 and GNP/RT-44 composites.

From the analysis of the endothermic curve for RT-44, the onset melting temperature (T_{om}) and endset melting temperature (T_{em}) were determined to be 40.36 °C and 44.73 °C, respectively, while the latent heat (H_m) was measured as 239.2 J/g. When 1%, 3% and 5% GNP is added to RT-44, T_{om} and T_{em} temperatures and H_m values are given quantitatively in Table 2. It is seen that GNP addition does not affect the melting onset and melting endset temperatures. On the other hand, it was determined that the latent heat of melting decreased depending on the amount of GNP addition. For example, the latent heat of melt for 5% GNP/RT-44 composite was measured as 226.3 J/g, which is a deterioration of 5.4% compared to RT-44. Essentially, this is an expected result due to the mixture of a material with high energy storage capability and a material with low energy storage capability. Similar results regarding the decreasing of the latent heat of melting with the addition of nanoparticles to the PCM have been reported in the literature. For example, Chen et al. [36], reported that when 5% GNP was added to paraffin with a latent heat of 144 J/g, the reduction in the latent heat of melting was approximately 16%. In this case, the partly lower latent heat of the paraffin employed may have resulted in a more pronounced reduction. However, the loss in latent heat is negligible in the face of the considerable improvement in thermal conductivity achieved with GNP doping.

Table 2. DSC properties of RT-44 and GNP/RT-44 composites.

Composite	T_{om} (°C)	T_{em}(°C)	H_m (J/g)
RT-44	40.26	44.73	239.2
1% GNP/RT-44	40.18	44.76	237.7
3% GNP/RT-44	40.11	44.81	235.4
5% GNP/RT-44	40.34	44.63	226.3

In the next phase of the study, performance tests were carried out to evaluate the effect of the PCM thickness of the PCM surrounding the resistance on the thermal protection. Acrylic tubes of three different diameters were used to create PCM thicknesses of 6 mm, 9 mm and 11 mm around the resistance.

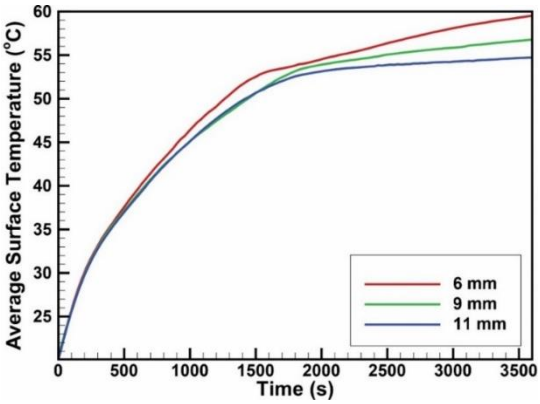

Figure 6. Variation of average surface temperature at different PCM thicknesses.

Figure 6 illustrates the variation in the mean surface temperature of the resistance over time for PCM thicknesses of 6, 9 and 11 mm. The reduction in temperature rise resulting from an increase in PCM thickness provides evidence that the thermal protection performance will be enhanced with greater PCM thickness. Below 40.26 °C, the temperature rise during sensible heat storage of PCM is almost independent of PCM thickness. Above 44.73 °C, it is determined that PCM thickness affects thermal protection as the PCM becomes liquid. The reason for this is that the conduction-dominant heat transfer mechanism (heat transfer is mostly by conduction) is effective in solid PCM and the convection-dominant (heat transfer is mostly by convection) heat transfer mechanism is effective in liquid PCM. It is seen that increasing the PCM thickness in a liquid state, where the convection-dominant heat transfer mechanism is effective, significantly reduces the temperature rise. In case of using 11 mm PCM thickness, the temperature remains almost constant from 1500th second. In other words, increasing the PCM thickness cannot have an extra effect. For this reason, it was deemed appropriate to use 11 mm as the optimum PCM thickness in the study. In their numerical study, Dincer et al. [38] concluded that the optimum PCM thickness around the li-ion cell is 9 mm in terms of maximum surface temperature.

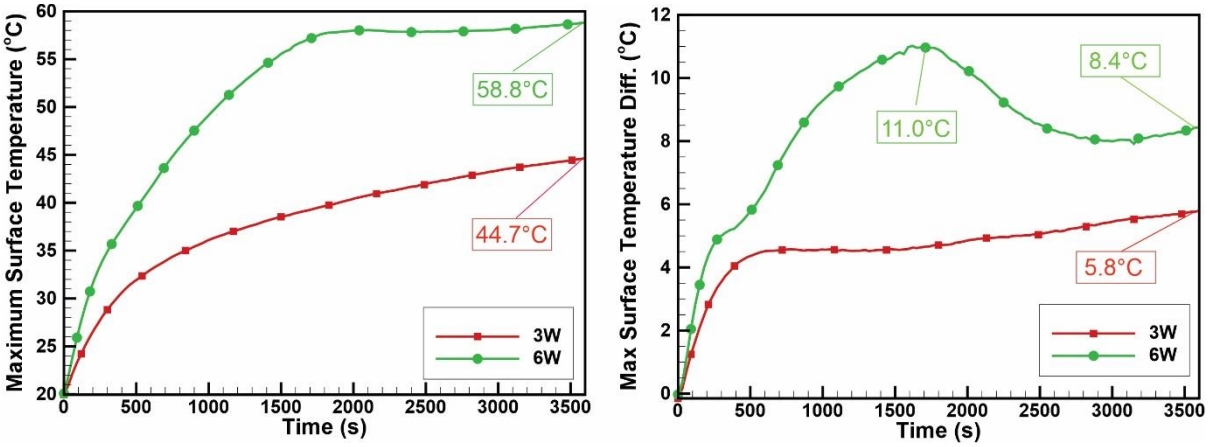

Figure 7. Variation of Maximum Temperature and Maximum Temperature Difference with time for RT-44.

The thermal protection performance of 3 W and 6 W heat-emitting resistances with 11 mm thick RT-44 is evaluated in Figure 7, based on the criteria of maximum surface temperature and maximum surface temperature difference. The upper region of the resistance is the maximum and the lower region is the minimum temperature region. With the onset of phase change, a decrease in density occurs in the liquid state as the temperature rises. This situation allows the low density hot liquid to move upwards. In other words, buoyancy movements start with the exposure of the liquid to temperature increase. As a result of the continuous upward

movement of heat by buoyancy movements, a significant temperature difference occurs between the upper and lower region of the resistance. Due to the low thermal conductivity of RT-44 organic PCM, a rapid temperature increase occurs initially on the surface of the resistor due to the inability to transfer the heat released in the resistor to the inner region of the PCM. In other words, the principal mechanism of heat transfer in the resistance/RT-44 system is conduction.

At 3 W heating power, the maximum temperature was observed to reach 44.7 °C at the end of 3600 seconds. It can thus be stated that the phase change is still in its initial stage, as the melting endset temperature of RT-44 has not yet been reached. In such a case, it can be stated that the energy released from the heat source is fully stored by the PCM as sensible (heat storage based on temperature change) heat. The deceleration in temperature increases at 3 W heating power is attributable to the resistance/PCM system achieving thermal equilibrium with its surrounding environment. In terms of limiting the maximum temperature, it is a sufficient condition that the temperature value remains below 50 ºC. The maximum surface temperature difference exhibited a similar behavior, with a maximum temperature difference of 5.8 ºC at the end of 3600 seconds. Considering that the maximum surface temperature difference below 5 ºC on the thermally protected component is the expected performance criterion, it can be said that RT-44 thermal protection alone is not sufficient.

The conduction-dominant heat transfer mechanism, initially effective at 6 W heating power, facilitates a faster temperature rise due to the low PCM thermal conductivity and high heating rate. In addition, the liquid layer formed around the heating source with the onset of phase change has two effects that support the temperature increase in the maximum temperature region. The first of these is the decrease in the conduction rate due to the lower thermal conductivity of the liquid RT-44 (approximately 0.150 W/mK). In other words, due to the low thermal conductivity in the liquid state, the slowing of the heat transfer in the radial direction to the PCM depths of conduction causes the temperature increase on the resistance surface. The second is the transfer of heat to the upper region of the resistance due to the effect of upward buoyancy currents that start with the increase in the liquid layer thickness sufficiently. As a result of the mentioned effects, the temperature increase in the upper region leads to the expansion of the liquid RT-44. The gradual weakening of heat conduction and the strengthening of buoyancy currents ensure that the dominant heat transfer mechanism returns to convection. The fact that the temperature remains almost constant in the maximum temperature region, especially from 1500 seconds onwards, is an indication of this. Similar findings have been

reported in the literature. Wang et al. [39] reported that when the PCM melting front intersects the upper region of the enclosure wall, the heating power on the resistor is balanced and the temperature remains constant as a result of the acceleration of convective heat transfer between the resistor and the enclosure wall. At 6 W heating power, the maximum surface temperature was measured as 58.8 ºC at the end of 3600 seconds. Until the convection dominant heat transfer is effective, the maximum surface temperature difference increases continuously. So much so that the maximum surface temperature difference reaches up to 11 ºC at 1618 seconds. From this moment on, the temperature difference slows down significantly because the maximum temperature zone in the upper region of the resistor remains approximately constant and the minimum temperature zone in the lower region of the resistance continues to increase. At the end of 3600 seconds, the maximum temperature difference was measured as 8.4 ºC and it was determined that the power increase in the RT-44 thermal protection negatively affected the maximum surface temperature difference. It was determined that RT-44 thermal protection at 6 W heating power could not provide sufficient protection due to exceeding the maximum temperature and maximum temperature difference limit values (50 ºC and 5 ºC).

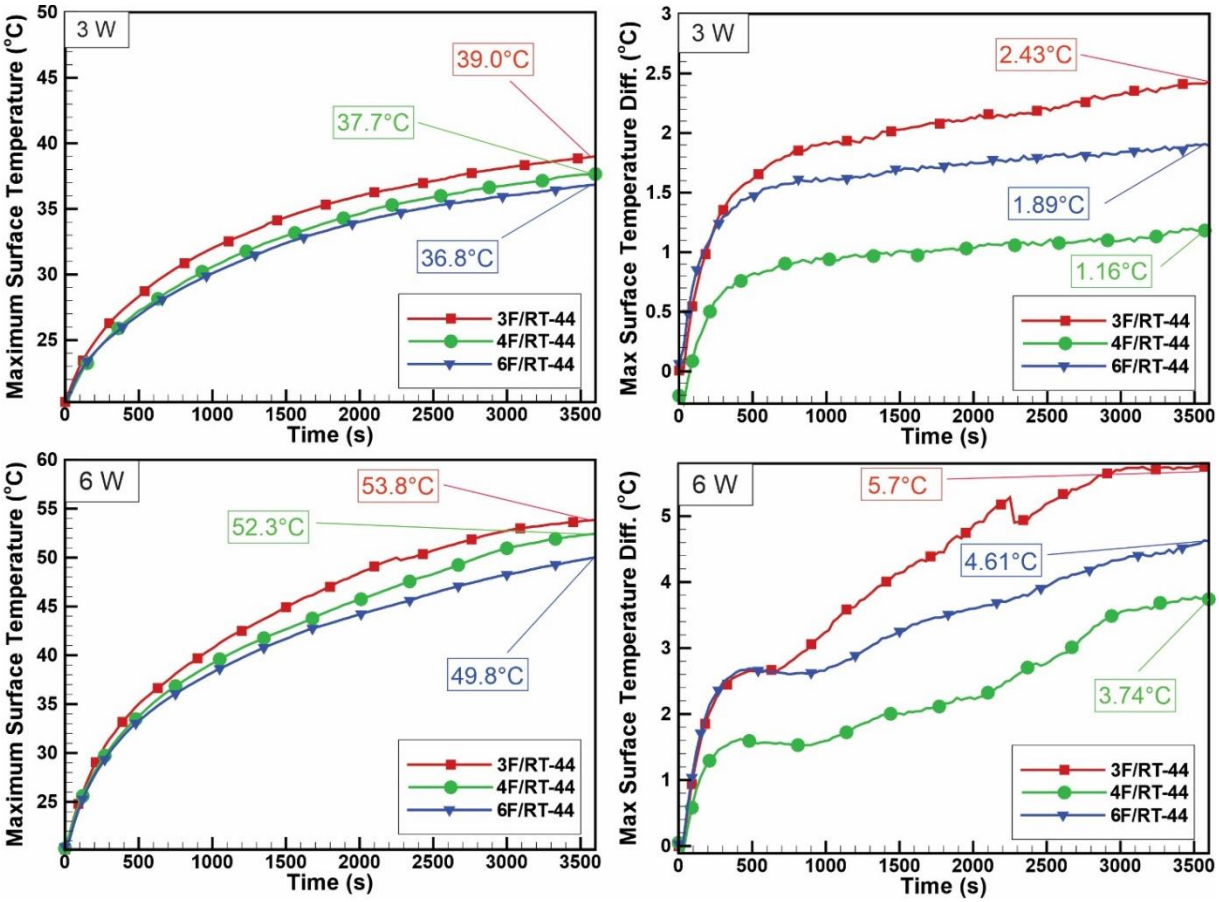

Figure 8. Variation of Maximum Temperature and Maximum Temperature Difference with time for Fins/RT-44 arrangements.

The thermal protection performances of the resistance/PCM system equipped with 3, 4, and 6 fins at 3 W and 6 W heating powers are evaluated in Figure 8 by considering the maximum surface temperature and maximum surface temperature difference criteria. At 3W heating power, it is observed that the time variation of the maximum temperature increase on the resistance slows down due to the increasing number of fins. In this case, it is clear that the heat released on the resistance is removed from the surface and transferred to the RT-44 by interacting with it in the radial direction along the fins. The aluminum fins with high thermal conductivity form thermal bridges for very fast heat transfer. Due to being below the RT-44 phase change temperature for 3600 seconds at 3 W heating power, the heat emitted from the resistance fin component is sensibly stored in the RT-44. At the end of 3600 seconds, the maximum temperature on the resistance in RT-44 thermal protection was 44.7 ºC, while the maximum temperatures for the 3, 4 and 6 fins resistance system were measured as 39.0 ºC, 37.7 ºC and 36.8 ºC, respectively. In this case, in terms of maximum surface temperature, RT-44 thermal protection with 3, 4 and 6 fins provide 12.8%, 15.7% and 17.7% performance improvements respectively. In terms of maximum surface temperature difference, it is an optimal design criterion that the temperature difference on the thermally protected component is below 5 ºC. It can be stated that the RT-44 thermal protections with 3, 4, and 6 fins have been effective in maintaining a maximum temperature difference below 5 °C. Additionally, the maximum surface temperature differences were found to be 2.4 ºC, 1.2 ºC and 1.9 ºC for the 3, 4 and 6-fins/RT-44, respectively. Given that the maximum surface temperature difference for the RT-44 thermal protection system is 5.8 ºC, the performance improvements of the 3, 4 and 6 fins/RT-44 system in comparison to the RT-44 thermal protection system are determined to be 58.6%, 79.3% and 67.2%, respectively.

At 6 W heating power, the deceleration in the maximum temperature increase depending on the number of fins is more pronounced. While the maximum temperature was 58.8 ºC at the end of 3600 seconds in RT-44 thermal protection, the maximum temperatures in RT-44 thermal protection with 3, 4, and 6 fins were measured as 53.8 ºC, 52.3 ºC and 49.8 ºC respectively. In other words, compared to RT-44, RT-44 thermal protection with 3, 4, and 6 fins provides 8.5%, 11.1%, and 15.3% performance improvement respectively. It was noted that the results obtained were compatible with those found in the literature. Wang et al.[39] found that the protection system with 4 copper fins at 6 W heating power reduced the maximum temperature by approximately 6 ºC. On the other hand, in this study, the maximum temperature limitation was measured as 6.5 ºC using aluminum fins under the same conditions. In terms of maximum

temperature difference, it is seen that the temperature difference has a continuously increasing trend. While the maximum surface temperature difference at the end of 3600 seconds in RT-44 thermal protection is 8.4 ºC, the maximum surface temperature differences in RT-44 protection systems with 3, 4, and 6 fins are measured as 5.7 ºC, 3.7 ºC and 4.6 ºC, respectively. In this case, it is determined that 3, 4, and 6 fins/RT-44 protections provide 32.1%, 56.0%, and 45.2% performance improvement, respectively, compared to RT-44 thermal protection.

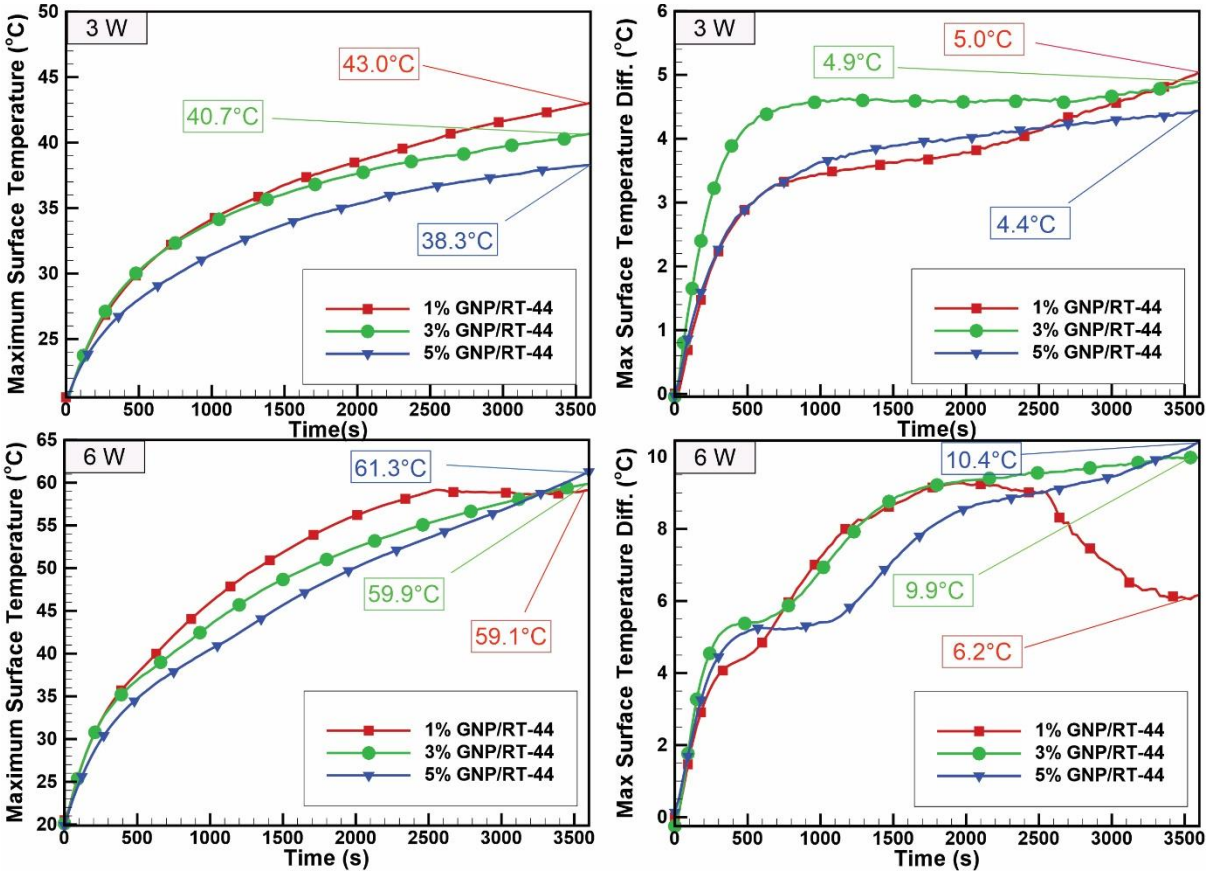

Figure 9. Variation of Maximum Temperature and Maximum Temperature Difference with time for GNP/RT-44 composites.

The thermal protection performances of RT-44 composites doped with 1%, 3%, and 5% GNP at 3 W and 6 W heating powers were evaluated in Figure 9 by considering the maximum surface temperature and maximum surface temperature difference criteria. At 3 W heating power, the rate of sensible heat storage of by RT-44 below the phase change temperature increases. For RT-44 composites doped with 1%, 3% and 5% GNP, the maximum surface temperatures at the end of 3600 seconds were measured as 43 ºC, 40.7 ºC and 38.3 ºC, respectively. In other words, it was determined that the thermal protection performances of 1%, 3% and 5% GNP doped RT-44 composites were improved by 3.8%, 8.9% and 14.3% compared to RT-44 thermal protection in terms of limiting the maximum surface temperature. It is seen

that GNP nanoparticle doping in RT-44 has a decreasing effect on the maximum surface temperature difference. While the maximum surface temperature difference at the end of 3600 seconds for RT-44 thermal protection was 5.8 ºC, the maximum surface temperature differences in RT-44 composites doped with 1%, 3% and 5% GNP nanoparticles were measured as 5.0 ºC, 4.9 ºC and 4.4 ºC, respectively. It was determined that the maximum surface temperature difference performances compared to RT-44 were improved by 13.8%, 15.5% and 24.1% in 1% GNP/RT-44, 3% GNP/RT-44 and 5% GNP/RT-44 composites respectively.

It can be said that the results obtained are compatible with the results for GNP/PCM thermal protection in the literature. Temel et al.[40] reported that the maximum temperature of 7% GNP/RT-44 composite was limited to 47 ºC as a result of 3600 seconds at 3.90 W heating power in a simulative battery pack. In this study, the maximum temperature was obtained as 38.3 ºC with 5% GNP/RT-44 at 3 W heating power for the same period, while in the other study the maximum temperature was measured as 47 ºC with 7% GNP/RT-44. This difference can be explained as follows; i) Higher heating power (3.90 W), ii) Contribution of neighboring cells to heating in battery pack, iii) 7% GNP/RT-44 composite suppresses natural convection movements more than 5% GNP/RT-44.

At 6 W heating power, the maximum temperature exhibits a lower temperature increase compared to RT-44 due to the thermal conductivity improvement effect provided by 1%, 3%, and 5% GNP doping by mass during conduction dominant heat transfer. For example, at the end of 1800 seconds, the maximum temperature on the resistance in RT-44 thermal protection was 57.68 ºC, while the maximum temperatures for RT-44 composites doped with 1%, 3%, and 5% GNP were measured as 54.67 ºC, 51.0 ºC and 48.45 ºC, respectively. In this case, at the end of 1800 seconds, it can be said that the thermal protection performances of 1% GNP/RT-44, 3% GNP/RT-44, and 5% GNP/RT-44 composites are 5.2%, 11.6%, and 16.0% better than RT-44, respectively. However, it is seen that the mentioned thermal protection improvement is lost with the transition to convection-dominated heat transfer. In fact, while the temperature increase remains constant from approximately 2000 seconds in RT-44, it remains constant after 2585 seconds in 1% GNP/RT-44. On the other hand, in RT-44 composites doped with 3% and 5% GNP, it is seen that there is no constant temperature change, on the contrary, the temperature continues to increase. The reason for this is that the viscosity increases as the GNP ratio doped into RT-44 increases. The inhibition of buoyancy-driven movements due to increased viscosity slows down the transfer of heat released on the resistance in the liquid phase where the convection dominant heat transfer mechanism is effective. In fact, during convection-

dominated heat transfer, heat transfer slows down because the positive effect of GNP addition above 3% on thermal conductivity is smaller than the negative effect due to the suppression of convection movements. In terms of maximum temperature protection, 3% GNP/RT-44 and 5% GNP/RT-44 composites perform worse than 1% GNP/RT-44 from 3292 and 3270 seconds respectively. At the end of 3600 seconds, the maximum temperature on the resistance in RT-44 thermal protection was 58.74 ºC, while the maximum temperatures for RT-44 composites doped with 1%, 3%, and 5% GNP were measured as 59.13 ºC, 59.88 ºC and 61.27 ºC, respectively. In this case, it can be said that the thermal protection performances of 1% GNP/RT-44, 3% GNP/RT-44 and 5% GNP/RT-44 composites deteriorated by 0.7%, 1.9% and 4.3% compared to RT-44 thermal protection. While the maximum surface temperature difference in RT-44 thermal protection at 6 W heating power was 8.4 ºC, the maximum surface temperature differences for 1% GNP/RT-44, 3% GNP/RT-44 and 5% GNP/RT-44 composites were measured as 6.2 ºC, 9.9 ºC and 10.4 ºC, respectively. In this case, in terms of maximum surface temperature difference, 1% GNP/RT-44 thermal protection shows 26.9% performance improvement compared to RT-44 thermal protection. On the contrary, 3% GNP/RT-44 and 5% GNP/RT-44 thermal protection show 17.9% and 23.8% worse performance respectively.

If convection-dominated heat transfer mechanism is dominant in RT-44 thermal protection, it is an advantage that the maximum temperature remains constant for a certain period of time. On the other hand, the increase in the temperature difference between the upper and lower region due to buoyancy currents is seen as a disadvantage. The addition of GNP in RT-44 has two effects on the thermal protection performance of the buoyancy currents due to the increase in viscosity. The fact that the amount of GNP doped into RT-44 causes an increase in viscosity in the liquid phase leads to the inhibition of natural convection movements. For this reason, the maximum surface temperature increases continuously when 3% and more GNP is added by mass. This means unfavorable performance in terms of maximum surface temperature. On the other hand, the addition of GNP also has the effect of reducing the maximum temperature difference. In addition to the drawback of increased viscosity, other drawbacks include nanoparticle production is still limited to laboratory scale, the high cost of nanoparticles, and their negative impact on living organisms. For these reasons, keeping the amount of GNP used small is a limiting criterion. Under these limitations, 1% GNP/6F/RT-44 and 3% GNP/6F/RT-44 thermal protection methods were also investigated as a hybrid thermal protection system based on the use of less GNP. However, it has been observed that there were no studies in the literature on the combined use of different protection systems. For this purpose,

maximum surface temperature and maximum surface temperature difference performance measurements of 1% GNP/6F/RT-44 and 3% GNP/6F/RT-44 hybrid thermal protection systems were performed and the results are given in Figure 10.

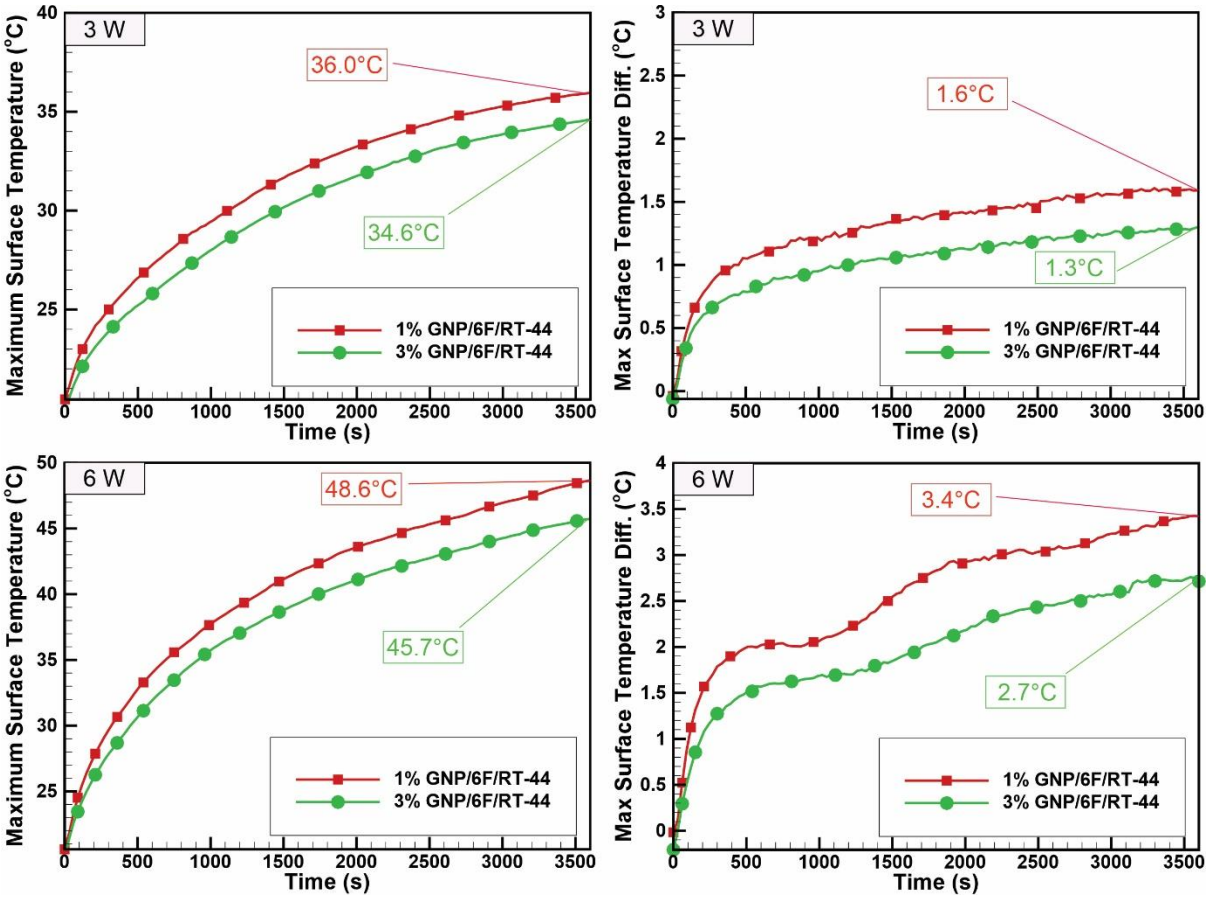

Figure 10. Variation of Maximum Temperature and Maximum Temperature Difference with respect to time for 1%GNP/6F/RT-44%, 3% GNP/6F/RT-44.

At the end of 3600 seconds at 3 W heating power, the maximum surface temperatures were 44.7 ºC, 36.8 ºC, 43.0 ºC, and 40.7 ºC for RT-44, 6F/RT-44, 1% GNP/RT-44 and 3% GNP/RT-44 thermal protections, respectively, while the maximum surface temperatures were 36 ºC and 34.6 ºC for 1% GNP/6F/RT-44 and 3% GNP/6F/RT-44 thermal protections, respectively. In this case, it was determined that the maximum surface temperature performances of 1% GNP/6F/RT-44 and 3% GNP/6F/RT-44 thermal protection could be improved by 19.5% and 22.6%, respectively, compared to RT-44 thermal protection. At the end of 3600 seconds at 3 W heating power, the maximum surface temperature differences were 5.8 ºC, 1.9 ºC, 5.0 ºC and 4.9 ºC for RT-44, 6F/RT-44, 1% GNP/RT-44 and 3% GNP/RT-44 thermal protections respectively, while the maximum surface temperature differences were 1.6 ºC and 1.3 ºC for 1% GNP/6F/RT-44 and 3% GNP/6F/RT-44 thermal protectors respectively. In other

words, compared to RT-44 thermal protection, 1% GNP/6F/RT-44 and 3% GNP/6F/RT-44 hybrid thermal protectors provide 72.4% and 77.6% performance improvement in terms of maximum surface temperature difference, respectively.

At the end of 3600 seconds at 6 W heating power, the maximum surface temperatures for 1% GNP/6F/RT-44 and 3% GNP/6F/RT-44 thermal protectors were measured as 48.6 ºC and 45.7 ºC, respectively. In this case, it was determined that 1% GNP/6F/RT-44 and 3% GNP/6F/RT-44 thermal protectors provided 17.3% and 22.3% improvement respectively compared to RT-44 thermal protection in terms of maximum surface temperature. At the end of 3600 seconds at 6 W heating power, the maximum surface temperature differences for 1% GNP/6F/RT-44 and 3% GNP/6F/RT-44 thermal protectors were measured as 3.4 ºC and 2.7 ºC, respectively. In other words, it was determined that 1% GNP/6F/RT-44 and 3% GNP/6F/RT-44 thermal protectors provided 41.4% and 53.4% improvement, respectively, compared to RT-44 thermal protection in terms of maximum surface temperature difference.

Table 3. Performance improvements over RT-44 thermal protection.

Composite	**Max. Temp. Enhancement (%)**	**Max. Temp. Enhancement (%)**	**Max. Temp.Diff. Enhancement (%)**	**Max. Temp. Diff. Enhancement (%)**
	3W	6W	3W	6W
RT-44	-	-	-	-
3F/RT-44	12.8	8.5	58.6	32.1
4F/RT-44	15.7	11.1	79.3	56.0
6F/RT-44	17.7	15.3	67.2	45.2
1% GNP/RT-44	3.8	-0.7	13.8	26.9
3% GNP/RT-44	8.9	-1.9	15.5	-17.9
5% GNP/RT-44	14.3	-4.3	24.1	-23.8
1% GNP/6F/RT-44	19.5	17.3	72.4	41.4
3% GNP/6F/RT-44	22.6	22.3	77.6	53.4

Table 3 summarizes the performance changes of all thermal protection methods with respect to RT-44 thermal protection. It has been determined that fin-added protections perform better than nanoparticle-added protections in terms of both maximum temperature and maximum temperature difference constraints. Nanoparticle-added protections are advantageous from the initial moment when heat conduction is dominant until the dominance of convection-dominated heat transfer, which is passed by the onset of buoyancy currents in the liquid phase. In the dominance of convection-dominant heat transfer, nanoparticle-protected thermal methods lose their advantages. With hybrid thermal protection systems, performance

improvements can be increased by 10%. It has been observed that the main contribution in hybrid thermal protection is provided by the fins and the fin/nanoparticle attachment does not create any synergistic effect. As a hybrid thermal protection system, it is determined that it is appropriate to limit the GNP mass fraction to a maximum of 3%. However, for longer protection times (>3600s), the GNP mass fraction should be kept low.

4 CONCLUSION AND SUGGESTIONS

Phase change material-based thermal protection of a heat-releasing system is compared in terms of PCM, fin/PCM, GNP/PCM, and fin/GNP/PCM composites and the results are given below.

- ✓ From the comparison of 6, 9, 11 mm PCM thicknesses in terms of maximum temperature criterion, it was concluded that 11 mm PCM thickness is the appropriate thickness.
- ✓ The thermal conductivities of GNP composites doped with 1%, 3% and 5% GNP were improved by 35.9%, 119.2% and 178.6%, respectively, in the solid phase. In the same case, the improvements obtained for the liquid phase were 18.5%, 55.6% and 89.5%, respectively.
- ✓ While the amount of GNP doped into RT-44 does not cause a significant change in melting temperatures, it causes a decrease in latent heat in proportion to the amount of GNP doped. For 5% GNP/RT-44 composite, this reduction is 5.4%.
- ✓ In RT-44 thermal protection, the maximum temperature and maximum temperature difference are 44.7 ^{o}C and 5.8 ^{o}C respectively in case of 3 W heat dissipation, while they are 58.8 ^{o}C and 8.4 ^{o}C respectively in the case of 6 W heat dissipation. In this case, considering that the maximum temperature and maximum temperature difference limit values are 50 ^{o}C and 5 ^{o}C, RT-44 thermal protection alone is not sufficient.
- ✓ Fin/RT-44, GNP/RT-44, and Fin/GNP/RT-44 composites provide sufficient thermal protection in terms of keeping the maximum temperature below 50 ^{o}C and the maximum temperature difference below 5 ^{o}C for 3600 seconds at 3 W heating power.
- ✓ At the end of 3600 seconds at 6 W heating power, 3F/RT-44, 4F/RT-44, and 6F/RT-44 thermal protectors have 8.5%, 11.1%, and 15.3% improvement performance over RT-44 thermal protection in terms of maximum temperature restriction, respectively.

Similarly, 3F/RT-44, 4F/RT-44, and 6F/RT-44 thermal protectors have 32.1%, 56.0%, and 45.2% performance improvement over RT-44 thermal protection in terms of maximum temperature difference restriction, respectively.

- ✓ 6F/RT-44 thermal protection provides successful thermal protection by keeping the maximum temperature at 49.8 ºC and the maximum temperature difference at 4.6 ºC after 3600 seconds at 6 W heating power.
- ✓ The addition of 1%, 3%, and 5% GNP to RT-44 creates an advantage during sensible heat storage and a disadvantage during latent heat storage in terms of thermal protection.
- ✓ At the end of 3600 seconds at 6 W heating power, 1% GNP/RT-44, 3% GNP/RT-44 and 5% GNP/RT-44 thermal protectors show 0.7%, 1.9% and 4.3% worse performance than RT-44 thermal protection in terms of limiting the maximum temperature, respectively. In terms of limiting the maximum temperature difference compared to RT-444 thermal protection, 1% GNP/RT-44 has 26.9% performance improvement, 3% GNP/RT-44 and 5% GNP/RT-44 have 17.9% and 23.8% performance deterioration respectively.
- ✓ There is no synergistic effect in the Fin/GNP/RT-44 hybrid thermal protection and the main contribution to the thermal protection performance is provided by the fins.
- ✓ Fin/GNP/RT-44 hybrid thermal protections have usability when the GNP mass fraction is kept below 3%. At the end of 3600 seconds at 6 W heating power, 1% GNP/6F/RT-44, 3% GNP/6F/RT-44 thermal protections provide 17.3% and 22.3% performance improvement over RT-44 thermal protection in terms of limiting the maximum temperature, respectively. Similarly, 1% GNP/6F/RT-44 and, 3% GNP/6F/RT-44 thermal protections provide 41.4% and 53.4% performance improvement over RT-44 thermal protection in terms of limiting the maximum temperature difference.

The most important disadvantage of further increasing the number of fins is known as weight increase. However, the increase in the number of fins also causes a decrease in the amount of PCM. When the weight increase is ignored, the evaluation of the positive effects of increasing the number of fins (decrease in the amount of PCM) in terms of thermal protection performance criteria can be carried out as a subject of future study.

Conflict of Interest Statement

There is no conflict of interest between the authors.

Statement of Research and Publication Ethics

The study is complied with research and publication ethics.

Artificial Intelligence (AI) Contribution Statement

This manuscript was entirely written, edited, analyzed, and prepared without the assistance of any artificial intelligence (AI) tools. All content, including text, data analysis, and figures, was solely generated by the authors.

Contributions of the Authors

The experimental studies of this study were carried out by Ahmet Can Çapar and Ümit Nazlı Temel. Data analysis and interpretations, manuscript writing and editing were performed by Ümit Nazlı TEMEL.

REFERENCES

[1] A. E. Kabeel, A. Khalil, S. M. Shalaby, and M. E. Zayed, "Experimental investigation of thermal performance of flat and v-corrugated plate solar air heaters with and without PCM as thermal energy storage," *Energy Convers. Manag.*, vol. 113, pp. 264–272, 2016, doi: 10.1016/j.enconman.2016.01.068.

[2] P. Mihálka, C. Lai, S. Wang, and P. Matiaˇ, "Experimental investigation of the daily thermal performance of a mPCM honeycomb wallboard," vol. 159, pp. 419–425, 2018, doi: 10.1016/j.enbuild.2017.10.080.

[3] Y. Galazutdinova, S. Ushak, M. Farid, S. Al-Hallaj, and M. Grágeda, "Development of the inorganic composite phase change materials for passive thermal management of Li-ion batteries: Application," *J. Power Sources*, vol. 491, no. June 2020, 2021, doi: 10.1016/j.jpowsour.2021.229624.

[4] W. L. Cheng, B. J. Mei, Y. N. Liu, Y. H. Huang, and X. D. Yuan, "A novel household refrigerator with shape-stabilized PCM (Phase Change Material) heat storage condensers: An experimental investigation," *Energy*, vol. 36, no. 10, pp. 5797–5804, 2011, doi: 10.1016/j.energy.2011.08.050.

[5] K. Du, J. Calautit, P. Eames, and Y. Wu, "A state-of-the-art review of the application of phase change materials (PCM) in Mobilized-Thermal Energy Storage (M-TES) for recovering low-temperature industrial waste heat (IWH) for distributed heat supply," *Renew. Energy*, vol. 168, pp. 1040–1057, 2021, doi: 10.1016/j.renene.2020.12.057.

[6] D. Mondieig, F. Rajabalee, A. Laprie, H. A. J. Oonk, T. Calvet, and M. A. Cuevas-Diarte, "Protection of temperature sensitive biomedical products using molecular alloys as phase change material," *Transfus. Apher. Sci.*, vol. 28, no. 2, pp. 143–148, 2003, doi: 10.1016/S1473-0502(03)00016-8.

[7] V. Chinnasamy and H. Cho, "Thermophysical investigation of metallic nanocomposite phase change materials for indoor thermal management," *Int. J. Energy Res.*, vol. 46, no. 6, pp. 7626–7641, 2022, doi: 10.1002/er.7664.

[8] Ü. N. Temel and B. Y. Ç. İ. F. T. Ç. İ, "Determination of Thermal Properties of A82 Organic Phase Change Material Embedded with Different Type Nanoparticles List of Seymbols," pp. 75–85, 2018.

[9] L. W. Fan *et al.*, "Effects of various carbon nanofillers on the thermal conductivity and energy storage properties of paraffin-based nanocomposite phase change materials," *Appl. Energy*, 2013, doi: 10.1016/j.apenergy.2013.04.043.

[10] P. Goli, S. Legedza, A. Dhar, R. Salgado, J. Renteria, and A. A. Balandin, "Graphene-enhanced hybrid phase change materials for thermal management of Li-ion batteries," *J. Power Sources*, vol. 248, pp. 37–43, 2014, doi: 10.1016/j.jpowsour.2013.08.135.

[11] Y. Grosu *et al.*, "Hierarchical macro-nanoporous metals for leakage-freeygrosu@cicenergigune.com high-thermal conductivity shape-stabilized phase change materials," *Appl. Energy*, vol. 269, no. April, p. 115088, 2020, doi: 10.1016/j.apenergy.2020.115088.

[12] B. Zhang, Y. Zhang, K. Li, C. Ma, and B. Yuan, "Novel segregated-structure phase change materials with binary fillers and the application effect in battery thermal management," *J. Energy Storage*, vol. 54, no. June, p. 105336, 2022, doi: 10.1016/j.est.2022.105336.

[13] D. Zou *et al.*, "Preparation of a novel composite phase change material (PCM) and its locally enhanced heat transfer for power battery module," *Energy Convers. Manag.*, vol. 180, no. September 2018, pp. 1196–1202, 2019, doi: 10.1016/j.enconman.2018.11.064.

[14] G. Jiang, J. Huang, Y. Fu, M. Cao, and M. Liu, "Thermal optimization of composite phase change material/expanded graphite for Li-ion battery thermal management," *Appl. Therm. Eng.*, vol. 108, pp. 1119–1125, 2016, doi: 10.1016/j.applthermaleng.2016.07.197.

[15] M. Chen *et al.*, "Experimental study on the hybrid carbon based phase change materials for thermal management performance of lithium-ion battery module," *Int. J. Energy Res.*, vol. 46, no. 12, pp. 17247–17261, 2022, doi: 10.1002/er.8388.

[16] C. Ma, Y. Zhang, S. Hu, X. Liu, and S. He, "A copper nanoparticle enhanced phase change material with high thermal conductivity and latent heat for battery thermal management," *J. Loss Prev. Process Ind.*, vol. 78, no. January, p. 104814, 2022, doi: 10.1016/j.jlp.2022.104814.

[17] T. Xu, Y. Li, J. Chen, H. Wu, X. Zhou, and Z. Zhang, "Improving thermal management of electronic apparatus with paraffin (PA)/expanded graphite (EG)/graphene (GN) composite material," *Appl. Therm. Eng.*, vol. 140, no. May, pp. 13–22, 2018, doi: 10.1016/j.applthermaleng.2018.05.060.

[18] M. Chen *et al.*, "Preparation of thermally conductive composite phase change materials and its application in lithium-ion batteries thermal management," *J. Energy Storage*, vol. 52, no. PA, p. 104857, 2022, doi: 10.1016/j.est.2022.104857.

[19] X. Zhang, C. Liu, and Z. Rao, "Experimental investigation on thermal management performance of electric vehicle power battery using composite phase change material," *J. Clean. Prod.*, vol. 201, pp. 916–924, 2018, doi: 10.1016/j.jclepro.2018.08.076.

[20] Z. Wang, Z. Zhang, L. Jia, and L. Yang, "Paraffin and paraffin/aluminum foam composite phase change material heat storage experimental study based on thermal management of Li-ion battery," *Appl. Therm. Eng.*, vol. 78, pp. 428–436, 2015, doi: 10.1016/j.applthermaleng.2015.01.009.

[21] A. Hussain, C. Y. Tso, and C. Y. H. Chao, "Experimental investigation of a passive thermal management system for high-powered lithium ion batteries using nickel foam-paraffin composite," *Energy*, vol. 115, pp. 209–218, 2016, doi: 10.1016/j.energy.2016.09.008.

[22] Z. Rao, Y. Huo, X. Liu, and G. Zhang, "Experimental investigation of battery thermal management system for electric vehicle based on paraffin/copper foam," *J. Energy Inst.*, vol. 88, no. 3, pp. 241–246, 2015, doi: 10.1016/j.joei.2014.09.006.

[23] H. Dey, S. Pati, P. R. Randive, and L. Baranyi, "Effect of finned networks on PCM based battery thermal management system for cylindrical Li-ion batteries," *Case Stud. Therm. Eng.*, vol. 59, no. May, p. 104572, 2024, doi: 10.1016/j.csite.2024.104572.

[24] M. M. Heyhat, S. Mousavi, and M. Siavashi, "Battery thermal management with thermal energy storage composites of PCM, metal foam, fin and nanoparticle," *J. Energy Storage*, vol. 28, no. December 2019, 2020, doi: 10.1016/j.est.2020.101235.

[25] A. Moaveni, M. Siavashi, and S. Mousavi, "Passive and hybrid battery thermal management system by cooling flow control, employing nano-PCM, fins, and metal foam," *Energy*, vol. 288, no. May 2023, p. 129809, 2024, doi: 10.1016/j.energy.2023.129809.

[26] Z. Wang, H. Zhang, and X. Xia, "Experimental investigation on the thermal behavior of cylindrical battery with composite paraffin and fin structure," *Int. J. Heat Mass Transf.*, 2017, doi: 10.1016/j.ijheatmasstransfer.2017.02.057.

[27] S. F. Hosseinizadeh, F. L. Tan, and S. M. Moosania, "Experimental and numerical studies on performance of PCM-based heat sink with different configurations of internal fins," *Appl. Therm. Eng.*, vol. 31, no. 17–18, pp. 3827–3838, 2011, doi: 10.1016/j.applthermaleng.2011.07.031.

[28] A. Acır and M. Emin Canlı, "Investigation of fin application effects on melting time in a latent thermal energy storage system with phase change material (PCM)," *Appl. Therm. Eng.*, vol. 144, no. September, pp. 1071–1080, 2018, doi: 10.1016/j.applthermaleng.2018.09.013.

[29] L. L. Tian, X. Liu, S. Chen, and Z. G. Shen, "Effect of fin material on PCM melting in a rectangular enclosure," *Appl. Therm. Eng.*, vol. 167, no. April 2019, 2020, doi: 10.1016/j.applthermaleng.2019.114764.

[30] M. J. Huang, P. C. Eames, B. Norton, and N. J. Hewitt, "Natural convection in an internally finned phase change material heat sink for the thermal management of photovoltaics," *Sol. Energy Mater. Sol. Cells*, vol. 95, no. 7, pp. 1598–1603, 2011, doi: 10.1016/j.solmat.2011.01.008.

[31] P. Ping, R. Peng, D. Kong, G. Chen, and J. Wen, "Investigation on thermal management performance of PCM-fin structure for Li-ion battery module in high-temperature environment," *Energy Convers. Manag.*, vol. 176, no. August, pp. 131–146, 2018, doi: 10.1016/j.enconman.2018.09.025.

[32] G. Türkakar and İ. Hoş, "Numerical investigation of lithium-ion battery thermal management using fins embedded in phase change materials," *J. Fac. Eng. Archit. Gazi Univ.*, vol. 38, no. 2, pp. 1105–1116, 2023, doi: 10.17341/gazimmfd.762563.

[33] F. Bahiraei, A. Fartaj, and G. A. Nazri, "Experimental and numerical investigation on the performance of carbon-based nanoenhanced phase change materials for thermal management applications," *Energy Convers. Manag.*, vol. 153, no. August, pp. 115–128, 2017, doi: 10.1016/j.enconman.2017.09.065.

[34] C. V. Hémery, F. Pra, J. F. Robin, and P. Marty, "Experimental performances of a battery thermal management system using a phase change material," *J. Power Sources*, vol. 270, pp. 349–358, 2014, doi: 10.1016/j.jpowsour.2014.07.147.

[35] U. Nazli, T. Kutlu, S. Murat, and P. Kerim, "Transient thermal response of phase change material embedded with graphene nanoplatelets in an energy storage unit," *J. Therm. Anal. Calorim.*, vol. 133, no. 2, pp. 907–918, 2018, doi: 10.1007/s10973-018-7161-7.

[36] Y. J. Chen, D. D. Nguyen, M. Y. Shen, M. C. Yip, and N. H. Tai, "Thermal characterizations of the graphite nanosheets reinforced paraffin phase-change composites," *Compos. Part A Appl. Sci. Manuf.*, 2013, doi: 10.1016/j.compositesa.2012.08.010.

[37] S. Kim and L. T. Drzal, "High latent heat storage and high thermal conductive phase change materials using exfoliated graphite nanoplatelets," *Sol. Energy Mater. Sol. Cells*, vol. 93, no. 1, pp. 136–142, 2009, doi: 10.1016/j.solmat.2008.09.010.

[38] N. Javani, I. Dincer, G. F. Naterer, and B. S. Yilbas, "Heat transfer and thermal management with PCMs in a Li-ion battery cell for electric vehicles," *Int. J. Heat Mass Transf.*, vol. 72, pp. 690–703, 2014, doi: 10.1016/j.ijheatmasstransfer.2013.12.076.

[39] Z. Wang, H. Zhang, and X. Xia, "Experimental investigation on the thermal behavior of cylindrical battery with composite paraffin and fin structure," *Int. J. Heat Mass Transf.*, vol. 109, pp. 958–970, 2017, doi: 10.1016/j.ijheatmasstransfer.2017.02.057.

[40] U. N. Temel, "Passive thermal management of a simulated battery pack at different climate conditions," *Appl. Therm. Eng.*, vol. 158, no. May, p. 113796, 2019, doi: 10.1016/j.applthermaleng.2019.113796.